Chapter

CARBON–COATED FUNCTIONALIZED MAGNETIC NANOPARTICLES FOR BIOMEDICAL APPLICATIONS

Mercedes Arana[1], Paula Bercoff[1], Silvia Jacobo[2] and Marcela Rodríguez[3]

[1]Facultad de Matemática, Astronomía y Física,
Universidad Nacional de Córdoba. IFEG, Conicet. Córdoba, Argentina
[2]LAFMACEL, Facultad de Ingeniería, Universidad de Buenos Aires.
INTECIN, Conicet. Buenos Aires, Argentina
[3]Facultad de Ciencias Químicas, Universidad Nacional de Córdoba.
INFIQC, Conicet. Córdoba, Argentina

ABSTRACT

Carbon–coated magnetite nanoparticles (NPs) were synthetized by the mechanochemical method with hematite as precursor and amorphous carbon as inorganic reductor. After 18 hours of milling in an inert atmosphere, a nanocomposite material of magnetite and carbon was obtained.

Structural and magnetic properties of the NPs were investigated by X-ray diffraction (XRD), scanning electron microscopy (SEM), transmission electron microscopy (TEM), energy dispersive X-ray spectroscopy (EDS) and vibrating sample magnetometry. XRD patterns, refined with the Rietveld method, show that magnetite is present in

samples milled from 6 hours onward and that after milling for 18 hours and annealing in Ar, the sample contains a single crystalline phase. Magnetization curves for samples with different milling times show saturation magnetization values that range from 34.1 emu/g after 1 h to 78.0 emu/g after 18 h. Coercive fields are about 500 Oe for all samples. TEM studies reveal that the samples are made of amorphous carbon clusters with magnetite NPs of 20 nm.

The obtained NPs, associated to electrochemical transducers, show an improved enhancement of the charge transfer for redox processes involving different bioanalytes. Thus, these NPs offer unique properties as a catalyst in biosensing strategies for the electrochemical detection of high-impact markers and the development of theranostics smart-devices for biomedical applications.

Index Terms—Carbon, coatings, magnetic nanoparticles, hydrogen peroxide, biosensor

I. INTRODUCTION

The physical and biological sciences share a common interest in nanoscale, since integrating biology and nanomaterials may improve different fields of science and technology. Nanomaterials and nanotechnology are widely applied in biomedicine, especially in the areas of biomedical diagnosis, drugs and implants [1]. The applications of biomedical nanotechnology outside the body include biosensors and biochips and inside the body include targeted drugs delivery, implantation of insulin pumps and gene therapy [2].

Nanoscience and nanotechnology comprise different biomedical applications for magnetic nanomaterials. Most of the biomedical applications of magnetic nanomaterials are based on their specific characteristics.

Though magnetic nanoparticles with different compositions, sizes and shapes have been developed for biomedical applications, the most frequently used magnetic materials are maghemite (γ-Fe_2O_3) and magnetite (Fe_3O_4). [3–9].

Nowadays, there is a rising demand for biosensors with high sensitivity and reliability, fast response and excellent selectivity. Biosensors have found versatile applications in the field of environmental control, hazard material, detection, pharmaceutics and clinical diagnostics. A common biosensor works as a biospecific surface interacting with a particular analyte, and generating detectable signals, such as electrochemical, optical, piezoelectrical and thermal

responses. The enzyme glucose oxidase (GOx) has been the most widely used biorecognition element in glucose biosensors [10]. GOx catalyzes the oxidation of glucose to gluconolactone and this, in turn, reduces the oxygen to hydrogen peroxide. The main challenge when designing electrochemical glucose biosensors is the development of strategies that allow an important decrease in the high overvoltage required for the oxidation and reduction of hydrogen peroxide (H_2O_2) at carbon electrodes in order to improve H_2O_2 quantification [11].

Comba et al [11–13] reported the advantages of using carbon paste electrodes modified with magnetite and iron nanoparticles in glucose biosensors. These authors found that sensor sensitivity is related to magnetite content. However, high NPs contents promote a highly resistive behavior due to the low–conductive nature of magnetite. These considerations led us to infer that magnetite-carbon interface could play an important role in the biosensor response. We decided to prepare carbon–coated magnetite nanoparticles in order to explore this idea.

Mechanical milling is recognized as an effective way of producing solid–state chemical reactions at low temperatures. This is a well–known process, with the first publication dating back to some decades ago [14], that induces chemical reactions in powder precursors during the collisions with the grinding media [15]. Mechanical milling can be classified as mechanical grinding, mechanical alloying, and mechanochemical synthesis in relation to the precursors, the milling parameters and the structural and chemical changes that occur during the milling. Mechanical grinding in a high–energy ball mill favors the formation of fine (nanosized) particles, while the chemical composition of precursors changes as a result of mechanically induced solid state reaction [15, 16].

Mechanochemical reactions are characterized by a large negative free energy change at room temperature and therefore they are thermodynamically favorable at room temperature [17, 18]. The preparation of soft ferrites by mechanosynthesis involves chemical precursors such as mixtures of oxides, chlorides and/or metals that react either during milling or during subsequent heat treatment, to form a new product or composite powder. In particular, it is possible to produce an 80 – 95% of spinel phase from a stoichiometric mixture of simple oxides as precursors, in a high–energy ball mill (in dry or wet media), while the single ferritic phase is usually obtained only with a posterior thermal annealing [19].

The applications of mechanochemistry include exchange reactions, reduction/oxidation reactions, decomposition of compounds, and phase

transformations. Let M be a pure metal, R a reductant and MO the corresponding metal oxide reduced by R. Thus, the exchange reactions in mechanochemistry can be represented by an equation of the type $MO + R \rightarrow M + RO$.

In this work we report the preparation of carbon–coated magnetite NPs by mechanosynthesis, and their structural and magnetic characterization (part of which was previously reported in [20]). These NPs were included within carbon paste electrodes in order to explore their analytical performance towards hydrogen peroxide reduction and to evaluate their response as a glucose biosensor.

II. EXPERIMENTAL

Magnetite (Fe_3O_4) NPs were synthesized by the mechanochemical method in a *Fritsch Pulverisette 7* high–energy ball mill. The structural characterization of the samples was performed by X ray diffraction (XRD) with a Phillip X'Pert diffractometer, with Cu–K_α radiation, and Rietveld refinement using *FullProf Suite* software. The magnetic properties were determined with a Lake Shore 7300 vibrating sample magnetometer (VSM) at room temperature and with a maximum applied field of 1200 kA/m (1.5 kOe). The size distribution and the morphology of samples were investigated with a field emission scanning electron microscope (FE–SEM) *SIGMA, Zeiss* and with a high resolution transmission electron microscope (HR–TEM) *Philips CM 200 (200kV)* that is equipped with a LaB6 emission filament which operates at 200 keV.

The electrochemical measurements were performed with a TEQ_04 potentiostat. The electrodes were inserted into the cell (BAS, Model MF–1084) through holes in its Teflon cover. A platinum wire and Ag/AgCl, 3 M KCl (BAS, Model RE–5B) were used as counter and reference electrodes, respectively. All potentials are referred to the latter. A magnetic stirrer provided the convective transport during the amperometric measurements. The electrochemical characterization of magnetite NPs was performed using a composite carbon paste electrode (CPE). The CPE was prepared in a regular way by mechanically mixing graphite powder (70.0% w/w) and mineral oil (30.0% w/w) in an agate mortar for 30 min. CPEs containing magnetite NPs (CPE–NPs) and commercial magnetite microparticles (100–500 nm) (CPE–MPs) were prepared in a similar way, mixing first the magnetite NPs or commercial magnetite MPs with mineral oil for 3 min, followed by the

incorporation of the graphite powder and mixing for additional 30 min. In the case of the enzymatic electrode, GOx and magnetite NPs were first mixed with the mineral oil for 10 min before incorporating the graphite powder and then mixed for additional 30 min. A portion of the resulting paste was packed firmly into the cavity (3 mm diameter) of a Teflon tube (3 mm diameter). The electric contact was established through a stainless steel screw. A new surface was obtained by smoothing the electrode onto a weighing paper before starting every new experiment. Cyclic voltammetric experiments were performed in 0.050 M buffer phosphate solution pH 7.40 as supporting electrolyte. The amperometric measurements were conducted in a stirred 0.050 M buffer phosphate solution pH 7.40 by applying the desired working potential and allowing the transient current to decay to a steady–state prior to the addition of the analyte and subsequent current monitoring. All the electrochemical measurements were performed at room temperature.

III. SYNTHESIS AND STRUCTURAL CHARACTERIZATION

High-energy Ball Milling

Hematite (Fe_2O_3) and activated carbon were used as precursors in a 4:1 mass ratio according to the following reaction:

$$3Fe_2O_3 + 10C \rightarrow 2Fe_3O_4 + CO + 9C \quad (1)$$

As reaction (1) indicates, extra C is introduced in the vials so that a carbon excess remains in the sample even after the hematite reduction process has finished, covering the formed magnetite particles. An inert atmosphere had to be used in the milling vials to avoid secondary oxidation processes.

The milling was performed at 700 rpm, with a ball/powder mass ratio of 35, in stainless steel vials with WC balls and Ar atmosphere. Every synthesis parameter was chosen after several tests and previous studies.

The samples that result from the milling are labeled CHt where *t* is the milling time in hours and takes the values 1, 2, 3, 6, 12 and 18.

Structural Characterization and Thermal Treatments

X ray diffraction patterns of hematite used as precursor and those of the resulting powders from the milling are shown in Figure 1.

From Figure 1, it is evident that the expected chemical reaction (1) starts at t = 6 h, but hematite is still present in the powder even after milling for 18 hours, indicating that the reaction is not complete. Activated carbon is amorphous; therefore, no reflections arising from this phase are expected with this technique.

In order to get rid of the remaining hematite in the samples and avoid further milling, the samples were annealed in Ar for 2 h at 500 ^{o}C. This temperature was carefully selected to prevent a significant particle growth as well as C evaporation [21] while promoting hematite reduction.

The resulting powders after annealing were labeled CHtT, being t the milling time in hours. X ray diffraction patterns for these samples are shown in Figure 2. Sample CH18T shows only magnetite reflections.

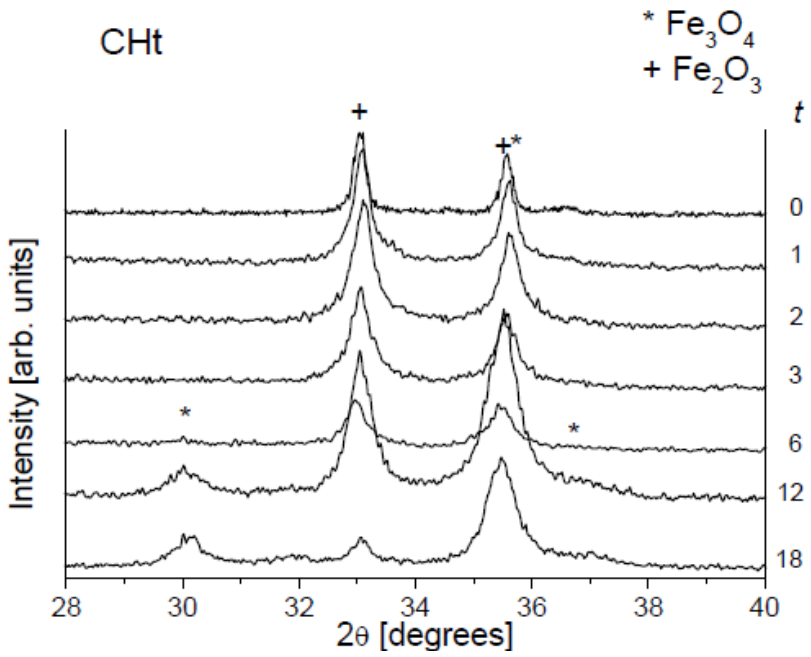

Figure 1. X ray diffraction patterns for samples milled from 1 to 18 h and as milled hematite.

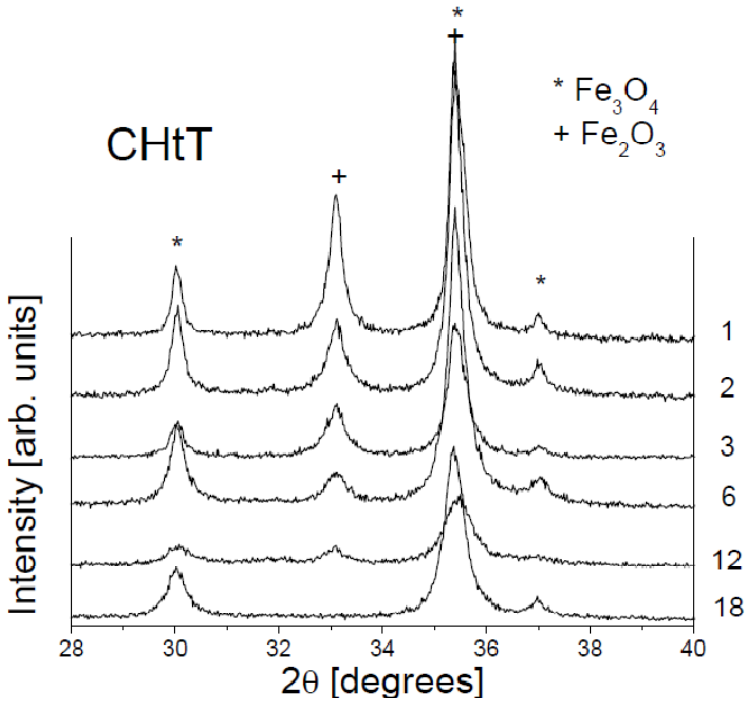

Figure 2. X ray diffraction patterns for samples milled from 1 to 18 h and annealed for 2 h at 500ºC, in Ar atmosphere.

Rietveld Analysis

X ray diffraction patterns were refined with the Rietveld method. Figure 3 shows the fitting of the corresponding spectra of samples CH1T, CH3T and CH18T.

The conventional Rietveld *R*–factors (Chi^2, GoF and R_{Bragg} for each crystalline phase) for XRD refinements of samples CHtT, for all the milling times are presented in Table I, while the structural parameters values of magnetite for: cell parameter *a*, cell volume *V*, density ρ , crystallite size $D_{crystal}$ and phase content of each sample *P* obtained from Rietveld refinement data are shown in Table II.

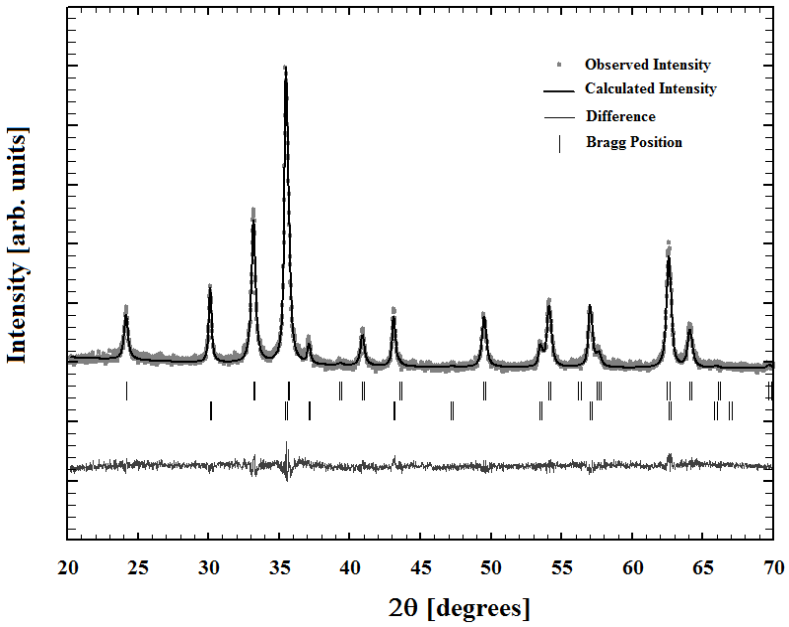

(a)

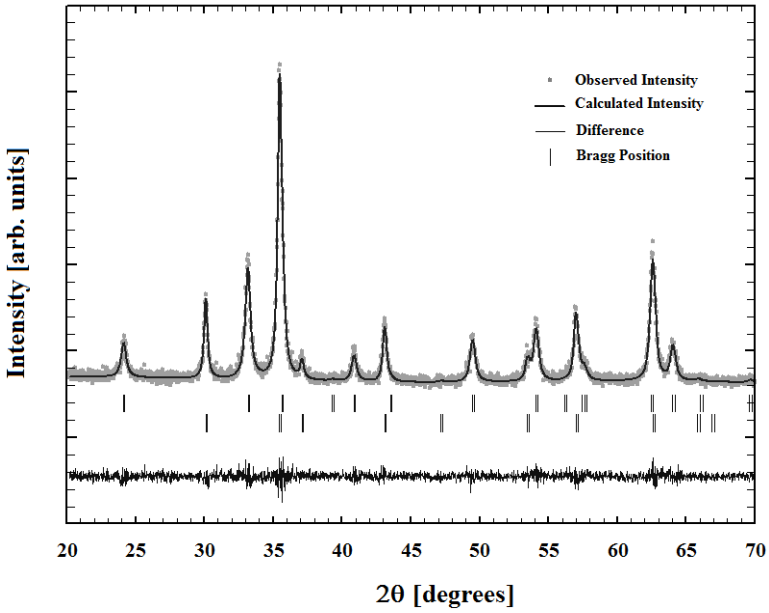

(b)

Figure 3. (Continued).

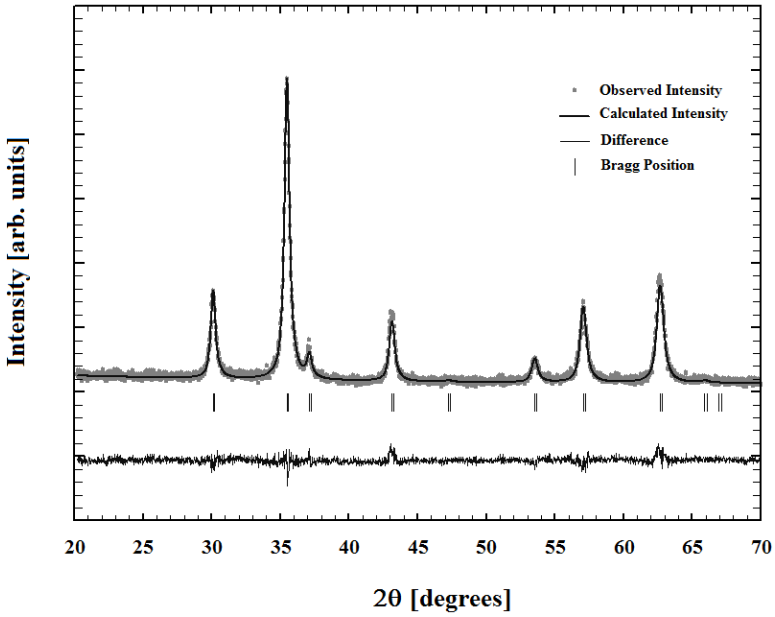

(c)

Figure 3. Rietveld refinements of the XRD pattern of samples CH1T (a), CH3T (b) and CH18T (c). Only magnetite reflections (vertical lines) are present in the pattern of sample CH18T. The dots are experimental data, the dark line is the theoretical pattern and the line below is the diference between experimental and theoretical data; vertical lines indicate the Bragg reflections.

Table I. Conventional Rietveld R-factors for samples CHtT

t	Chi^2	GoF	R_{Bragg}	
			Fe_2O_3	Fe_3O_4
CH1T	1.26	11.708	6.78	4.45
CH3T	1.13	4.511	4.33	2.73
CH6T	1.22	9.860	7.10	4.10
CH12T	1.55	24.326	26.0	10.60
CH18T	1.14	6.361	-	4.77

Even when the Rietveld method is quite accurate for determining crystallographic parameters and phases, it has proven to be rather tricky when an amorphous material is present in the sample. So, even when obtaining values of Chi^2 around 1 in every case, the overall quality parameter is high

(indicating not a good overall fit). In order to take the amorphous fraction into account, a different approach to the refinement must be addressed. However, the parameters obtained for the crystalline phases (hematite and magnetite, in this case) are reliable.

The cell parameter of magnetite slightly changes with the milling time. This change can be attributed to the strains which are generated in the synthesis process due to the impacts of the mill balls with the powder. Besides, the cell volume is affected with the milling time in a similar way.

It is clear from Table II that the interplanar distance of magnetite disminishes when the milling time increases from 1 to 18 h, taking values from 0.4720 to 0.4716 Å, respectively. The density of ferritic phase remains almost constant, with changes of the order of the accuracy of the calculation method and with values ranging from 5.21 to 5.23 g/cm^3.

Table II. Rietveld refinement parameters for samples CHtT

Sample	a [±0.0001Å]	d [±0.0002Å]	V [±0.001Å^3]	ρ [±0.01g/cm^3]	$D_{crystal}$ [±1nm]	P [%] Fe_2O_3	P [%] Fe_3O_4
CH1T	8.3879	0.4720	590.1388	5.212	43	56.6	43.4
CH3T	8.3895	0.4721	590.4822	5.213	28	51.0	48.8
CH6T	8.3872	0.4719	589.9957	5.216	27	20.1	79.9
CH12T	8.3803	0.4716	588.5320	5.225	11	20.3	79.7
CH18T	8.3813	0.4716	588.7602	5.224	20	0.0	100.0

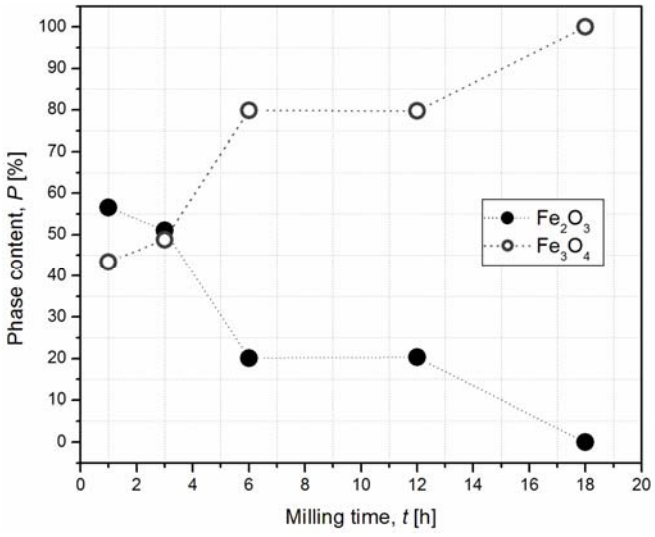

Figure 4. Hematite and magnetite content in the samples, as a function of milling time.

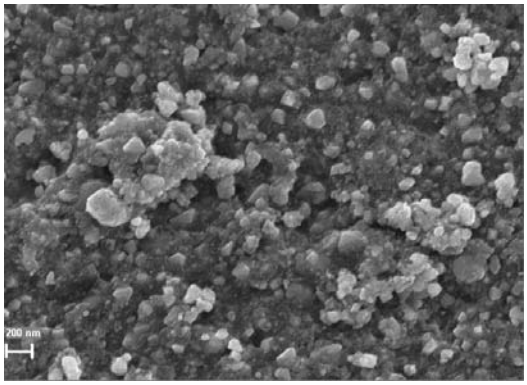

a)

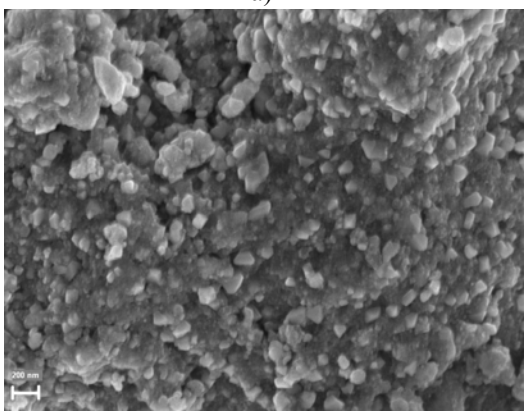

b)

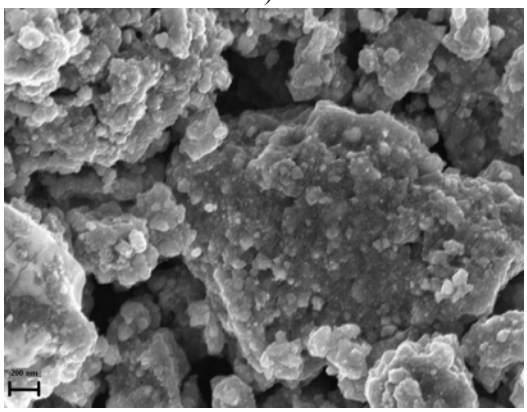

c)

Figure 5. (Continued).

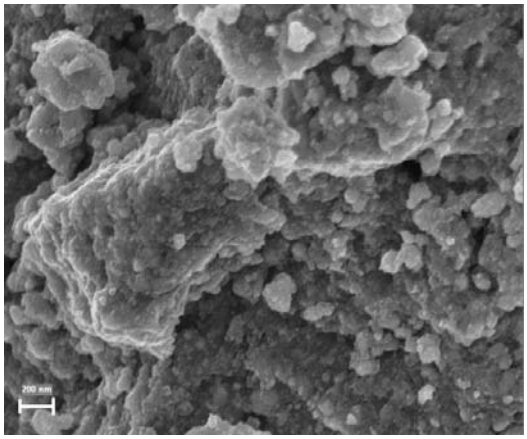

d)

Figure 5. SEM images for samples CHtT, for *t*=1 (a), 2(b), 3(c) and 6h (d).

Crystal size decreases from 43 to 11 nm for magnetite in samples milled from 1 to 12 h, and there is a small increase after 18 h of milling. This increase can be explained with the disappearance of hematite, which tends to prevent crystal growth [22].

The phase content P, as a function of milling time is presented in Figure 4. The reduction of hematite to magnetite as a function of milling time is evident, and is complete after 18 hours.

SEM and TEM Characterization

Scanning electron micrographs (SEM) show that that the particles are nanosized (see Figure 5) and appear in the powders as single particles and clusters.

Figure 6 shows secondary electron (a) and a backscattered electron (b) images of sample CH18T. In backscattered electron images, elements with a higher atomic number Z appear brighter than elements with lower Z. The comparison of figures 6 a and b indicates that nanometric crystals of ferrite are uniformly inmersed in carbon. This was further confirmed by transmission electron microscopy (TEM), which was also used to investigate the samples. In order to do so, the powders were dispersed in ethyl alcohol. Afterwards, small drops were deposited on ultrathin carbon support films (of the order of 4 nm thickness) which are then deposited on Cu grids and loaded in the TEM

holder. High resolution transmission electron microscopy (HRTEM) images show that sample CH18 is composed of nanosized particles, surrounded by carbon (see Figure 7), accordingly with SEM results. In the images presented in Figure 7, both hematite and magnetite can be identified with the different d-spacings of the crystalline planes, as indicated by the arrows. The size distribution is Gaussian–shaped. The particle size (D_P) distribution in the inset shows that the average particle size from TEM (D_{PT}) is 11 nm.

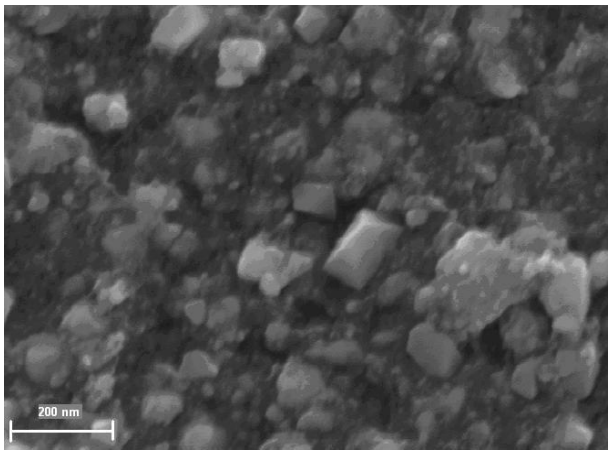

a)

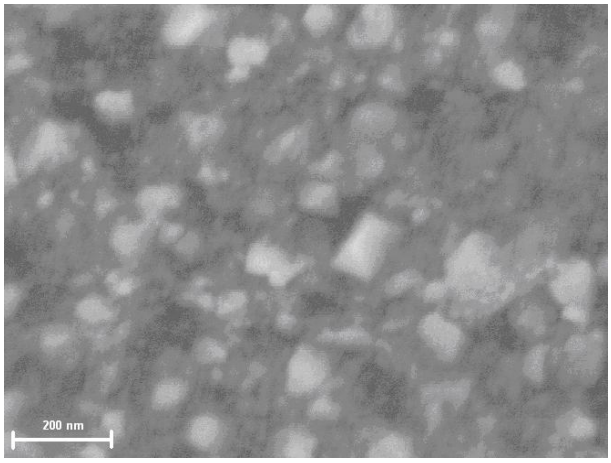

b)

Figure 6. SEM micrographs of sample CH18T. a) Secondary electrons image. b) Backscattered electrons image.

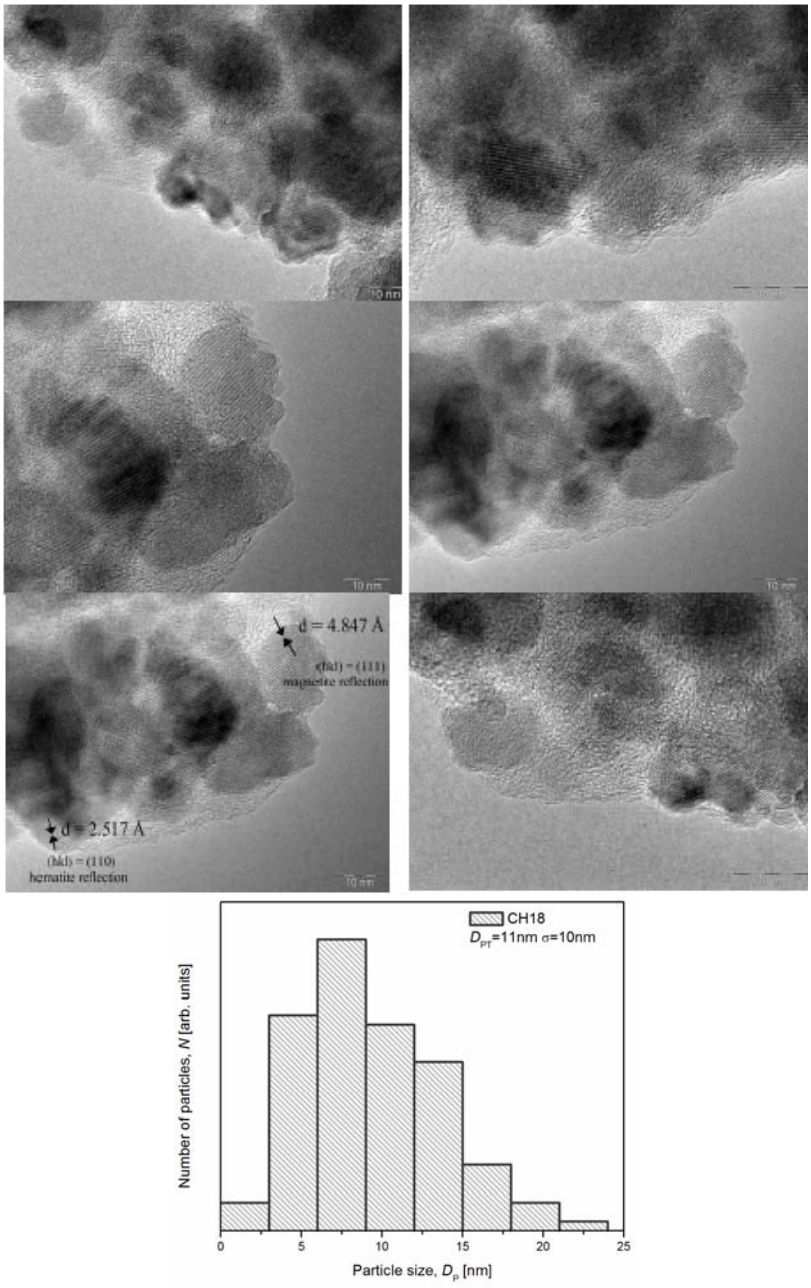

Figure 7. HRTEM images of sample CH18. The inset shows the particle size distribution.

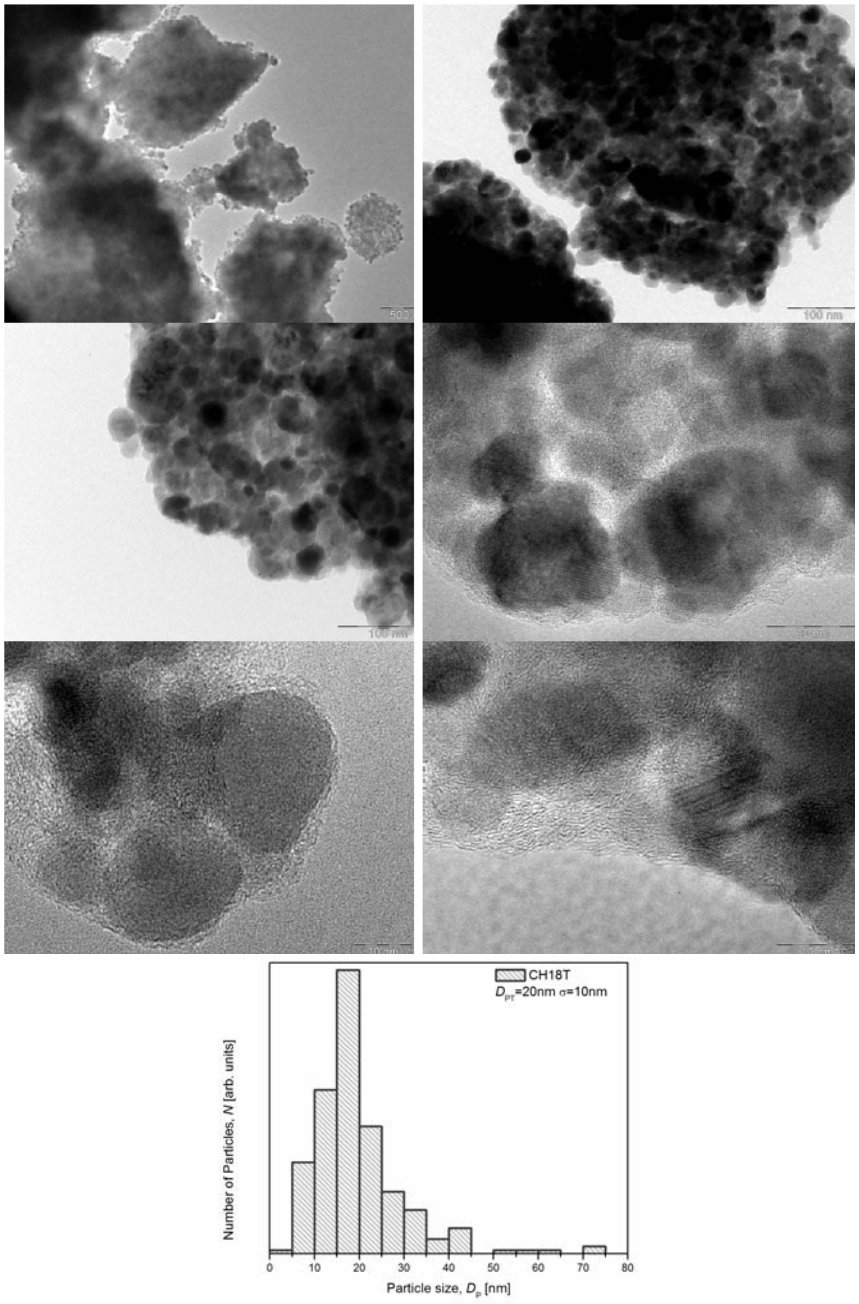

Figure 8. TEM and HRTEM images of sample CH18T. The inset shows the particle size distribution.

In Figure 8, TEM and HRTEM images of sample CH18T also show crystalline particles coated with the amorphous phase of carbon. Only one d–spacing value was identified, asociated to magnetite. The inset shows a Log–normal size distribution. This fact, together with the result from XRD indicates the existence of single–phase Fe_3O_4 NPs. The secondary phase –hematite– reduces completely to magnetite, and the thermal treatment promotes the growth of magnetite crystals from an average particle size D_{PT} = 11 nm (sample CH18) to 20 nm (sample CH18T).

Magnetic Characterization

The specific magnetization (σ) as a function of the applied magnetic field (H) for samples CHt and CHtT was measured and it is presented in Figures 9 and 10, respectively.

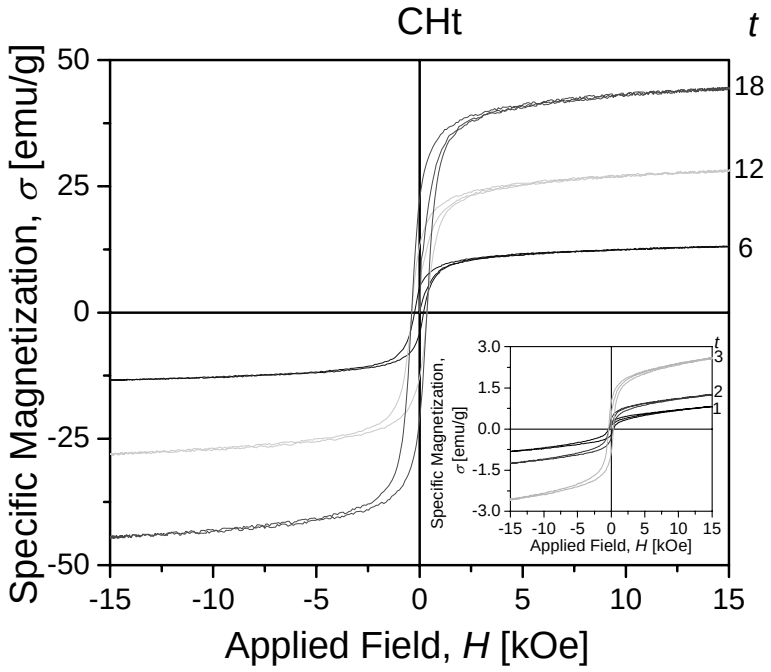

Figure 9. σ vs. H curves for samples CHt for t = 6, 12 and 18 h. The inset shows σ vs. H curves for samples CHt, for t =1, 2 and 3 h.

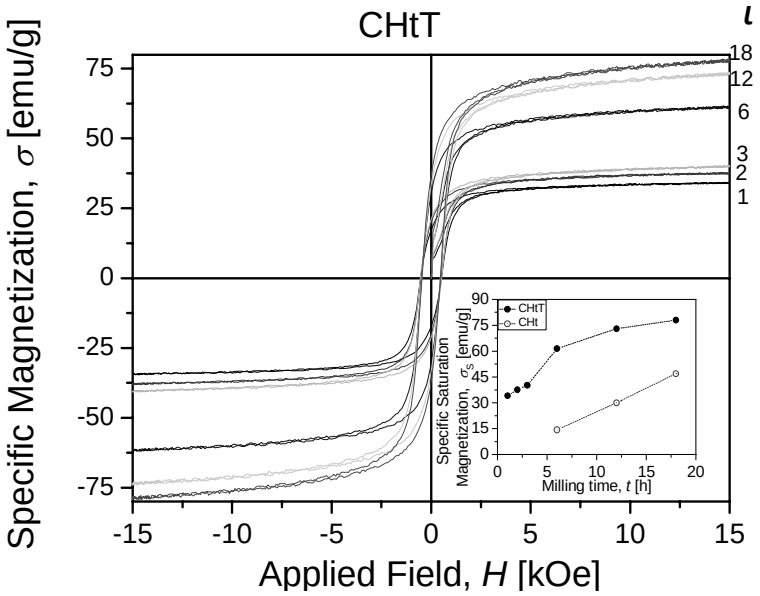

Figure 10. σ vs. H curves for samples CHtT. The inset shows σ_S values as a function of t for samples CHt and CHtT.

While the σ vs. H curves of samples CHt (for t = 1, 2 and 3 h) do not saturate and present low σ values, a significant increase in σ is observed when increasing the milling time from 1 to 3 hours (see the inset of Figure 9). This effect is due to the increase of the magnetite percentage with milling time. Samples milled from 6 to 18 hours do show a ferrimagnetic behavior (see Figure 9) as it is expected from the results obtained by XRD (Figure 1), where magnetite starts to appear after 6 h of milling and increases with milling time, t.

On the other hand, all the σ vs. H curves of samples CHtT show a typical ferrimagnetic behavior (Figure 10).

The specific saturation magnetization (σ_S) of these samples takes the values presented in the inset of Figure 10, where the σ_S values range from 34.1 emu/g after 1 h to 78.0 emu/g after 18 h (single–phase sample).

The value of specific saturation magnetization for bulk magnetite σ_S', is 92 emu/g [23], which is comparable to the specific saturation magnetization of sample CH18T (78.0 emu/g). The difference can be attributed to the fact that sample CH18T contains a fraction of carbon (non–magnetic material) apart from magnetite, so that σ_S is reduced. Besides, magnetization of a nanosized powder is usually reduced with respect to bulk magnetization values because

of surface effects; in this case, the superficial chemical bonds are bound to be broken by the milling process and the annealing temperature is not high enough to restore them.

In every case, coercive fields are about 500 Oe. The powders display rather high coercivity values and a slow approach to saturation, indicating that the nanoparticles aggregate in clusters (as confirmed by SEM and TEM) with a wide dispersion of cluster dimension.

Chantrell *et al.* [24] introduced a mathematical expression for determining the average particle size D_{PC} of a particulate system (and the corresponding standard deviation δ_C) using the magnetic parameters corresponding to σ vs. H curves, under the assumption of spherical particles with a Log–normal distribution. It is clear from the inset of Figure 8 that our systems fulfills this hypothesis; therefore Chantrell's expression can be used in this work.

Let T_r be the room temperature at the moment of the VSM measurement, χ_i the initial susceptibility, M_S the sample saturation magnetization, M'_S the bulk saturation magnetization and H_C the coercive field. Then D_{PC} and δ_C can be calculated according to [24]:

$$D_{PC} = \left[\frac{18 k_B T_r}{\pi M_S} \sqrt{\frac{\chi_i}{3 M'_S H_C}} \right]^{1/3}, \tag{2}$$

$$\delta_C = \frac{1}{3} \cdot \ln\left(\frac{3 \chi_i H_C}{M'_S} \right)^{1/3} \tag{3}$$

Using equations (2) and (3) with the corresponding error propagation, data from the measured σ vs H curves of Fig. 11, and the sample density from the Rietveld refinements, the particle size of the magnetic nanoparticle results D_{PC} = (18±1)nm with a standard deviation δ_C=0.3.

IV. ELECTROCHEMICAL CHARACTERIZATION AND BIOMEDICAL APPLICATION

It is widely known that several kinds of nanomaterials exhibit enzyme–like activity in a wide range of nonphysiological conditions as extreme pH

values, high temperature or in the presence of inhibitors [25]. This type of functional nanomaterials, that could be named “artificial enzymes”, have attracted great attention in the last years due to several advantages as stability under harsh conditions and effective biocatalysis as replacement of natural enzymes. Magnetite NPs are not the exception since they have demonstrated intrinsic peroxidase–like activity and have been applied as peroxidase nanomimetics to detect a wide range of biomolecules [26–32].

In order to explore this concept and characterize the electrochemical behavior of the C–coated magnetite NPs, investigate their peroxidase–like biocatalysis and consider their application in biosensing strategies, a C–coated NPs–modified composite electrode (NPs/CPE) was used in this work. For this purpose, sample CH18T was used.

For the evaluation of the electrocatalytic response towards 0.010 M hydrogen peroxide by cyclic voltammetry, three composite electrodes were assayed and compared: bare CPE (a), 5.0 % w/w commercial magnetite microparticles (MPs)/CPE (b) and 5.0% w/w NPs/CPE (c) (Figure 11 a). As shown in the figure, there is an important decrease in the overvoltage for the electro–oxidation and mainly for the electro–reduction of hydrogen peroxide and a significant increase of the associated currents for 5.0% NPs/CPE as expected, compared to the poor electrochemical response at the bare electrode (CPE) [11, 33–36] and at 5.0% MPs/CPE [36].

At the 5.0% C-coated NPs/CPE, the reduction current starts to increase at potentials more negative than 0.200V, as expected according to the excellent electrocatalytic action of magnetite NPs towards the reduction of hydrogen peroxide [25, 32, 35]. It is important to remark that NPs also catalyzes the hydrogen peroxide oxidation, starting at more positive potentials than 0.300 V, although this effect is less pronounced than in the case of the reduction.

Thus, the preferential reduction of hydrogen peroxide at C–coated NPs/CPE, allows reaching low–potential values for the amperometric detection offering a good alternative for the selective enzymatic quantification of glucose. Therefore, –0.100 V was selected as working potential for further amperometric experiments. Figure 11 b depicts cyclic voltammograms obtained for 0.010 M hydrogen peroxide at CPE containing increasing amounts of C–coated magnetite NPs: 0.0 (A), 2.5 (B), 5.0 (C), 10.0 (D) and 20.0 (E) % w/w. As expected, there is an enhancement in the reduction currents for hydrogen peroxide with the amount of nanomaterial, whereas there is an important increase in the capacitive currents that can be seen more clearly at the 20.0 %NPs/CPE. This behavior is due to the nonconductive

nature of magnetite and a resistive behavior due to a poor agglutination of the composite matrix with high content of NPs, as was reported previously [11].

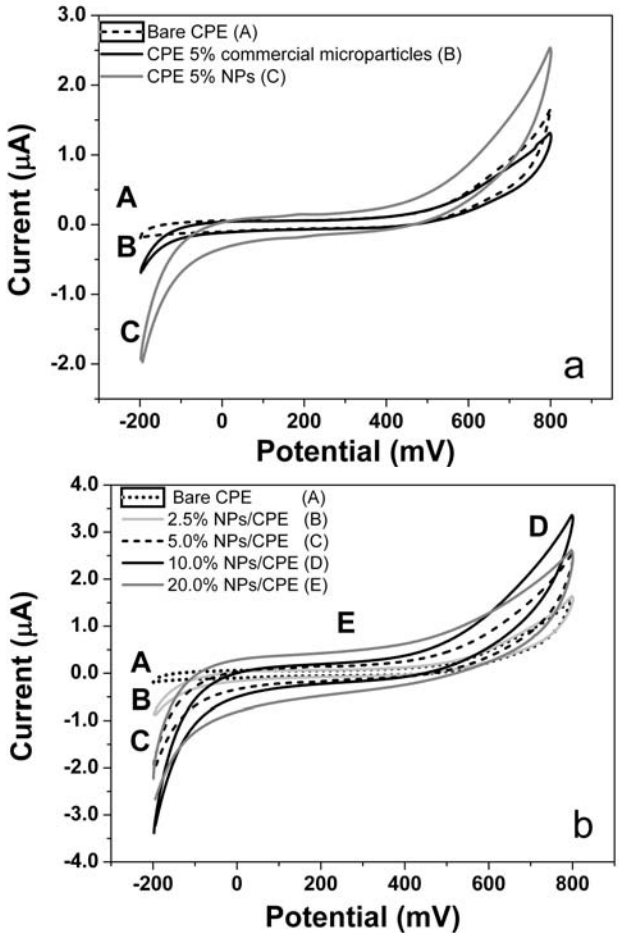

Figure 11. (a) Cyclic voltammograms for 0.010 M hydrogen peroxide at (A-dashed line) bare carbon paste electrode (CPE), at (B-solid black line) CPE modified with 5.0% w/w Fe_3O_4 microparticles (5.0% MPs/CPE) and at (C-solid grey line) CPE modified with 5.0% w/w C-coated Fe_3O_4 nanoparticles (5.0% NPs/CPE). Supporting electrolyte: 0.050 M phosphate buffer solution pH 7.40. Scan rate: 0.100 Vs^{-1}. (b) Cyclic voltammograms for 0.010 M hydrogen peroxide at CPE containing different percentages w/w of C-coated Fe_3O_4 nanoparticles: 0.0 (A-dotted line), 2.5 (B-light grey line), 5.0 (C-dashed line) 10.0 (D-solid grey line) and 20.0 (E-solid black line) % w/w NPs: Supporting electrolyte: 0.050 M phosphate buffer solution pH 7.40. Scan rate: 0.100 Vs^{-1}.

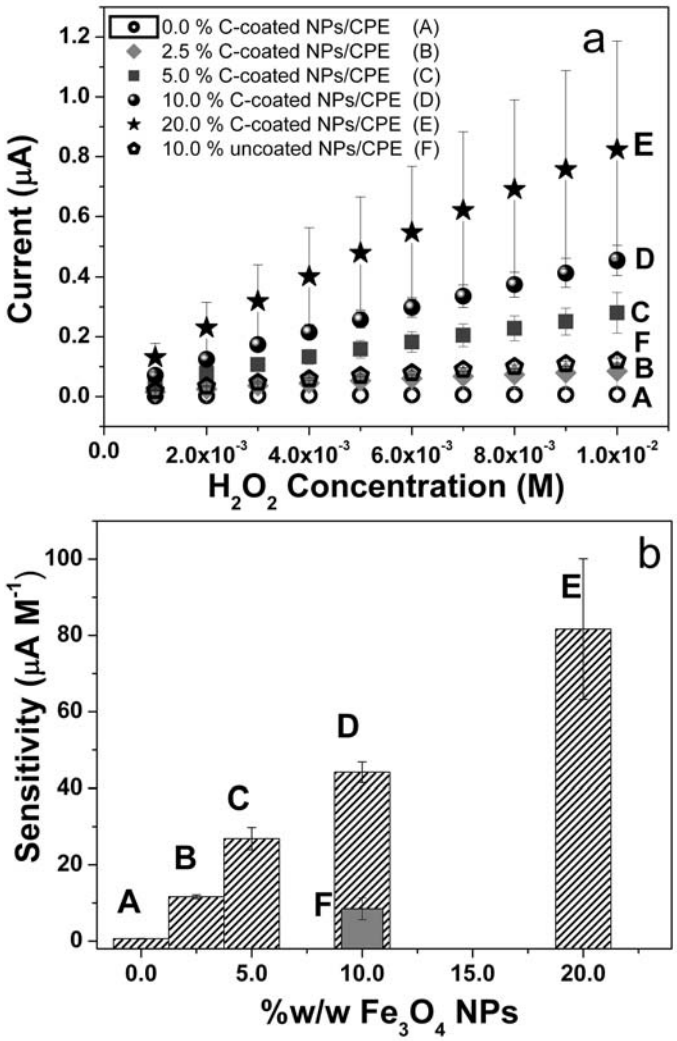

Figure 12. (a) Calibration plots obtained from amperometric experiments for successive additions of 1.0 x 10^{-3} M hydrogen peroxide performed at –0.100 V at CPE containing different percentages w/w of C-coated Fe_3O_4 nanoparticles: 0.0 (A), 2.5 (B), 5.0 (C), 10.0 (D), 20.0 (E) % w/w and uncoated Fe_3O_4 nanoparticles 10.0% w/w(F). Supporting electrolyte: 0.050 M phosphate buffer solution pH 7.40. (b) Sensitivity towards hydrogen peroxide obtained from amperometric experiments at -0.100 V (shown in a) at CPE containing different percentages w/w of C-coated Fe_3O_4 nanoparticles: 0.0 (A), 2.5 (B), 5.0 (C), 10.0 (D) and 20.0 (E) % w/w and uncoated Fe_3O_4 nanoparticles 10.0% w/w (F). Supporting electrolyte: 0.050 M phosphate buffer solution pH 7.40.

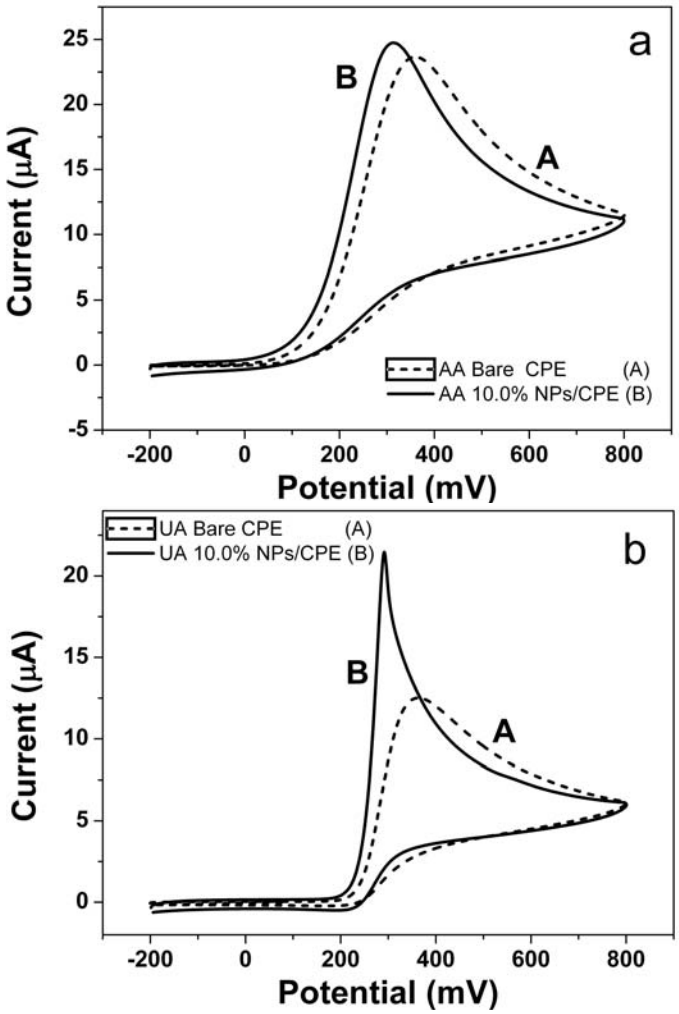

Figure 13. Cyclic voltammograms for (a) 1.0 x 10^{-3} M ascorbic acid (AA) and (b) 5.0 x 10^{-4} M uric acid (UA) at (A–dashed line) bare carbon paste electrode (CPE) and at (B–solid line) CPE modified with 10.0% w/w C–coated Fe_3O_4 nanoparticles (CPE 10.0% NPs). Supporting electrolyte: 0.050 M phosphate buffer solution pH 7.40. Scan rate: 0.100 Vs^{-1}.

The content of magnetite NPs in the composite material proved to be a very critical variable for the performance of the electrode. Figure 12a displays calibration plots obtained from amperometric recordings performed at –0.100 V for successive additions of 1.0 x 10^{-3} M hydrogen peroxide at CPE containing different percentages of C–coated magnetite NPs: 0.0 (A), 2.5 (B),

5.0 (C), 10.0 (D) and 20.0 (E) %w/w and 10.0 (F) %w/w uncoated–magnetite NPs, respectively. Figure 12b shows the corresponding sensitivity values towards hydrogen peroxide obtained from the calibration plots at –0.100 V (shown in Figure 12a).

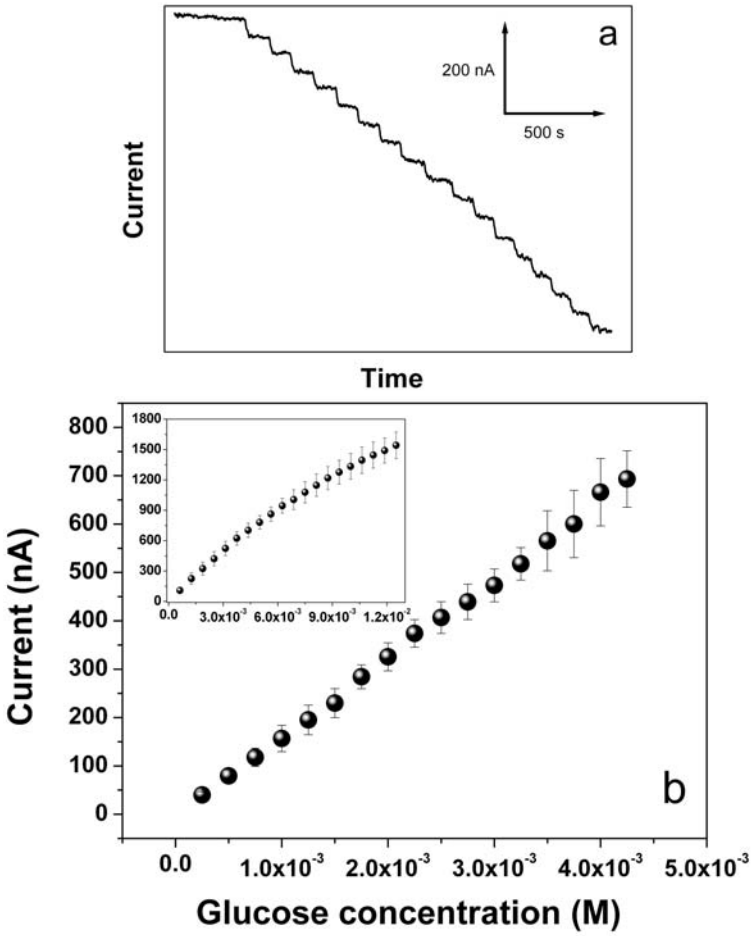

Figure 14. (a) Amperometric recordings for successive additions of 2.5 x 10^{-4} M glucose performed at -0.100 V at CPE containing 10.0 % w/w C–coated Fe_3O_4 nanoparticles and 5.0 % w/w GOx (10.0%C-coated NPs–5%GOx-CPE). Supporting electrolyte: 0.050 M phosphate buffer solution pH 7.40. (b) Calibration plot obtained from the amperometric recordings (shown in a). Inset: Calibration plot for successive additions of 6.25 x 10^{-4} M glucose in an extended range of concentrations. Working potential: -0.100 V. Supporting electrolyte: 0.050 M phosphate buffer solution pH 7.40.

The corresponding sensitivities are the following: (0.63 ± 0.07), (11.7 ± 0.5), (27 ± 3), (44 ± 3), (8 ± 2) x 10^1 μAM^{-1} for CPE containing 0.0; 2.5; 5.0; 10.0; and 20.0% w/w C–coated magnetite NP, respectively; while for 10.0% w/w uncoated magnetite NPs the sensitivity value found was (9 ± 3) μAM^{-1} . Analyzing the sensitivity values for CPE containing increasing amount of C–coated magnetite NPs, a linear relationship is obtained (with regression coefficient R^2= 0.997). As it was previously concluded from the cyclic voltammetric experiments (Figure 11 b), there is an important influence of the content of C–coated NPs on the sensitivity towards hydrogen peroxide. However, for 20.0% C–coated NPs/CPE, in addition to the important increase of the sensitivity, a very low reproducibility of the calibration curve is observed. This fact could be attributed to the agglutination difficulty of the composite matrix with the increasing content of magnetite NPs [35]. In view of these results, a 10.0% w/w C–coated magnetite NPs was selected as the optimum composition of the electrode material for a highly sensitive response. Likewise, the sensitivities towards hydrogen peroxide at 10.0% C–coated magnetite NPs/CPE and 10.0% uncoated magnetite NPs/CPE were compared (Figure 12a, curve D; Figure 12a, curve F; Figure 12b, column D and Figure 12b, column F) under the same experimental conditions. The sensitivity obtained for C–coated magnetite NPs is higher than the one for uncoated magnetite NPs by a factor of 5, demonstrating that the carbon surrounding provides a better environment for the catalytic activity and the electron transfer of magnetite NPs.

In the development of electrochemical biosensing strategies for blood glucose determination, a very remarkable aspect to take into account is the interference of easily oxidizable compounds, usually present in biological fluids, such as ascorbic acid (AA) and uric acid (UA). For this purpose, the catalytic activity of C–coated NPs/CPE towards the oxidation of these compounds was investigated. Figure 13 shows the typical voltammetric profiles obtained at 0.100 Vs^{-1} for 1,0 x 10^{-3} M AA (a) and for 1,0 x 10^{-3} M UA (b) at CPE (A–dotted line) and 10.0 % C-coated NPs/CPE (B–solid line). For C–coated NPs/CPE, there is a negative shift of 46 mV in the oxidation peak potential for AA and a negligible increase in the peak current from 23.6 to 24.7 μA. Moreover, for UA the catalytic effect is more evident, with a negative shift of 73 mV in the oxidation peak potential and an increase in the peak current from 12.5 to 21.6 μA (1.7 times). Nevertheless, although C–coated NPs reveal a slight catalysis for the oxidation of UA, the effect is not significant compared to the catalysis exhibited for hydrogen peroxide. Furthermore, at -0.100 V —the selected potential for amperometric detection

of hydrogen peroxide— there is no response to successive additions of AA and UA, even at higher concentrations than the physiological levels of these compounds (not shown), allowing a highly specific detection of hydrogen peroxide. Therefore, these results allow to conclude that C–coated magnetite NPs/CPE constitute a highly efficient system for the electrocatalytic reduction of hydrogen peroxide, making possible to consider its application in biosensing strategies for highly sensitive and selective glucose determination.

Upon the excellent performance of C–coated magnetite NPs/CPE towards hydrogen peroxide reduction and the remarkable selectivity in amperometric experiments, the following step was the design of a glucose biosensor by modifying 10.0% NPs/CPE with glucose oxidase (GOx) as biocatalyst. GOx catalyzes the oxidation of glucose to gluconic acid in presence of oxygen which is the natural regenerator of the enzyme active site, producing hydrogen peroxide after GOx regeneration. The amount of GOx within the composite has demonstrated to be an important variable in the development of the glucose biosensor, this amount is usually comprised between 5.0 and 10.0% [11, 33]. It is important to notice that for excessive amounts of GOx, commonly higher than 10.0% w/w, the oxygen consumption becomes more important, producing a shortening of the linear range [11, 34]. Therefore 5.0% w/w GOx was selected in order to compare the proposed magnetite NPs modified composite electrode with previous results [11]. In the designed biosensing strategy, the biosensor was obtained by dispersing 5.0% w/w of GOx within CPE modified with 10.0% w/w C–coated magnetite NPs. The reduction current of the hydrogen peroxide produced during the step of GOx regeneration obtained at –0.100 V, was taken as analytical signal. Figure 14a illustrates a current–time profile for successive additions of 2.5×10^{-4} M glucose, performed at –0.100 V at 5.0% GOx/10.0% C–coated NPs/CPE. A very fast and well–defined response is observed for each glucose addition. Similar amperometric experiments performed at 5.0% GOx/CPE at –0.100 V gave no response, as expected, due to the poor reduction of the hydrogen peroxide enzimatically generated at bare CPE [33]. Figure 14b displays a calibration plot obtained from the current–time profile (shown in Figure 14a) while the inset shows a calibration curve for successive additions of 6.25×10^{-4} M glucose performed at –0.100 V in an extended range of glucose concentration. A linear relationship between current and glucose concentration is obtained up to 7.5×10^{-3} M glucose (135 mg/dL), comprising the entirely physiological range and incipient pathological values. For higher glucose concentrations, the current increases non-linearly, as expected for biocatalyzed reactions. The average sensitivity obtained at –0.100 V was $(1.62 \pm 0.05) \times 10^{5}$

nAM^{-1} (R^2= 0.9992) and the quatification limit (taken as the smallest measured concentration) was 1.25 x 10^{-4} M. The kinetics parameters of the bioelectrode, K_M^{app} and I_{max}, were calculated by the Eadie–Hofstee plot obtained from the data of the calibration plot shown in Figure 14b (inset). The values obtained were the following: K_M^{app} : (0.02298 ± 0.0004) M and I_{max}: (4.39 ± 0,06) x 10^3 nA. The value found for the K_M^{app} falls within the range reported for K_M of GOx in homogeneous solution [37] and in the composite ceramic carbon matrix (K_M^{app} 20 ± 2 mol/L) [38], suggesting that the environment provided by C–coated magnetite NPs/composite matrix where GOx was immobilized is suitable for the biocatalytic activity of the enzyme.

The biosensor was further challenged by the addition of AA and UA. Figure 15 depicts the current–time profile at –0.100 V obtained after one addition of 5.0 x 10^{-4} M glucose, followed by successive additions of 2.0 x 10^{-5} M AA (a) and 4.0 x 10^{-5} M UA (b) up to achieve final concentrations of 2.0 x 10^{-4} M and 4.0 x 10^{-4}M, respectively. No interference signal in the presence of glucose was revealed for such concentrations, which are even higher than the maximum physiological levels found in human blood serum. This fact evidences the advantages of the preferential electrocatalytic detection of the enzymatically generated hydrogen peroxide, leading to a high sensitivity and an excellent selectivity.

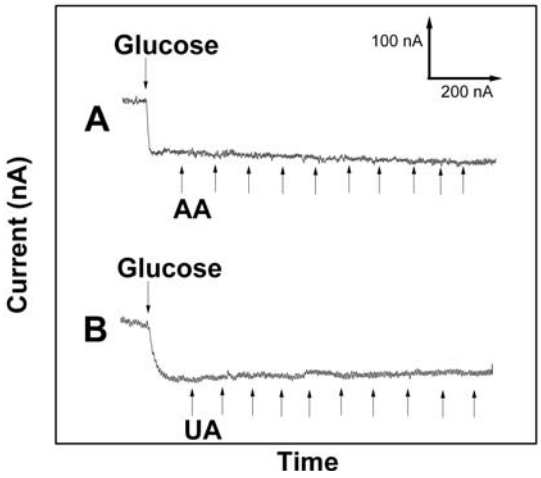

Figure 15. Current–time profiles performed at 10.0%C-coated NPs–5%GOx–CPE) for an addition of 5.0 x 10^{-4} M glucose and successive additions of (a) 2.0 x 10^{-5} M AA (up to reach a final concentration of 2.0 x 10^{-4} M and (b) 4.0 x 10^{-5} M UA (up to reach a final concentration of 4.0 x 10^{-4} M). Working potential: –0.100 V. Supporting electrolyte: 0.050 M phosphate buffer solution pH 7.40.

In order to evaluate the applicability of the bioelectrode for glucose practical determinations, 5.0% GOx/10.0% C–coated NPs/CPE was examined in the presence of human blood serum samples (Standatrol S–E–2, levels physiological N1 and pathological N2, Wiener Lab.). The glucose concentration obtained in the sample after 5 determinations were (91.6 ± 0.4) mg/dL for level N1 and (232 ± 6) mg/dL for level N2, while the glucose concentration reported by Wiener for levels N1 and N2 were 89 mg/dL and 238 mg/dL, respectively. These values gave a relative error of +2.8% and –2.6% for N1 and N2 samples, respectively, indicating the noteworthy performance of the proposed glucose biosensor for practical assays.

CONCLUSION

Stable carbon–coated magnetite NPs at room temperature were succesfully synthetized by the mechanochemical method and further thermal treatment at 500 ºC. A reduction of hematite to magnetite was induced by the mechanical process in which amorphous carbon was used in excess so as to remain covering the ferrite particles. The specific saturation magnetization of the resultant powder is very close to the bulk value. Crystal and particle sizes are the same (20 nm), indicating the obtention of single–crystal magnetite nanoparticles.

The use of C–coated magnetite nanoparticles for the development of an electrochemical glucose biosensor was proposed for the first time. C–coated magnetite NPs have demonstrated an excellent catalytic activity towards hydrogen peroxide enzimatically generated. This feature allowed quantifying glucose at potentials negative enough to avoid the interference of a large excess of easily oxidizable compounds or complex matrices as human blood serum. The resulting bioelectrode demonstrated an excellent analytical performance, comparable and even better than previous works using magnetite nanoparticles obtained by electrochemical synthesis with surfactants, as catalytic nanomaterial [11]. The simplicity of the preparation, the high sensitivity and selectivity, the excellent reproducibility of the proposed biosensor, and the excellent correlation of the results for blood human serum with those obtained using the spectrophotometric method, convert the proposed biosensor in a very good promise for practical applications in real biological systems. Based on the catalytic activity of C–coated magnetite nanoparticles and their known possibilities of functionalization, it is expected

that the surface modification of these nanoparticles with biomolecules will allow to have very efficient biosensors for a wide range of biomolecules.

This investigation is of particular significance for technological applications of C–coated NPs in biotechnology, environmental chemistry and biomedicine. It is expected that the synergic scientific contributions from different areas including chemistry, materials science, biology and clinical medicine would lead, in the near future, to further applications of modified magnetic nanomaterials in the development of smart–devices for theranostics purposes in the detection of high–impact markers of important pathological processes.

ACKNOWLEDGMENTS

This work was partially funded by Secyt-UNC, Conicet and ANPCyT.

REFERENCES

[1] Malsch, I. (2002). Biomedical applications of nanotechnology, *The Industrial Physicist*, 8(3), 15–17.

[2] Mehier–Humbert S. & Guy, R.H. (2005). Physical methods for gene transfer: improving the kinetics of gene delivery into cells, *Advanced Drug Delivery Reviews*, 57, 733–53.

[3] Podzus, P. E., Daraio M. E. & Jacobo S. E. (2009). Chitosan magnetic microspheres for technological applications: Preparation and characterization, *Physica B*, 404, 2710–2712.

[4] Aphesteguy, J. C., Jacobo, S. E., Schegoleva, N. N. & Kurlyandskaya G. V. (2010). Characterization of nanosized spinel ferrite powders synthesized by coprecipitation and selfcombustion method, *Journal of Alloys and Compounds*, 495 (2), 509–512.

[5] Sánchez, F., Mendoza Zélis, P., Pasquevich, G., Fernández van Raap, M., Stewart, S., Aphesteguy, J. & Jacobo, S. E. (2013). Structural and magnetic study of zinc- doped magnetic nanoparticles and ferrofluids for hyperthermia aplications. *Journal of Physica D: Applied Physics*. 46, 125006 (12pp).

[6] Bertoglio, P., Jacobo, S. E. & Daraio, M. E. (2010). Preparation and characterization of PVA films with magnetic nanoparticles: The effect of

particle loading on drug release behavior, *Journal Of Applied Polymer Science*, 115(3) 1859–1865.

[7] Albornoz, C., Sileo, E. E. & Jacobo, S. E. (2004). Magnetic polymers of maghemite (g-Fe2O3) and polyvinyl alcohol, *Physica B,* 354, 149–153.

[8] Albornoz, C. & Jacobo, S. E. (2006). Preparation of a biocompatible magnetic film from an aqueous ferrofluid. *Journal of Magnetism and Magnetic Materials*, 305(1), 12–15.

[9] François, N. J., Allo, S., Jacobo, S. E., Daraio, M. E. (2007). Composites of polymeric gels and magnetic nanoparticles: preparation and drug release behavior, *Journal of Applied Polymer Science*, 105, 647–655.

[10] [10] Lee, T. M. H. (2008). Over-the-counter biosensors: Past, Present, and Future *Sensors*, Vol 8(9), 5535–5559.

[11] [11] Comba, F. N., Rubianes, M. D., Cabrera, L., Gutiérrez, S., Herrasti, P. & Rivas, G. A. (2010). Highly sensitive and selective glucose biosensing at carbon paste electrodes modified with electrogenerated magnetite nanoparticles and glucose oxidase, *Electroanalysis*, 22(14), 1566–1572.

[12] Comba, F. N., Gutiérrez, F., Herrasti, P., Rubianes, M. D. & Rivas, G. A. (2012). Effect of the incorporation of proteins on the performance of carbon paste electrodes modified with electrogenerated magnetite nanoparticles towards the reduction of hydrogen peroxide, *Electroanalysis*, 24, 1541–1546.

[13] Comba, F. N., Rubianes, M. D., Herrasti, P., & Rivas, G. A. (2010), Glucose biosensing at carbon paste electrodes containing iron nanoparticles, *Sensors and Actuators B*, 149, 306–309.

[14] Lea, M. C. (1984). *Philosophical Magazine*, 34, 470–475.

[15] Suryanarayana, C. (2001). Mechanical alloying and milling, *Progress in Materials Science*, 46, 1–184.

[16] Takacs, L. (2002). Self-sustaining reaction induced by ball milling, *Progress in Materials Science*, 47, 355–414.

[17] Schaffer, G. B. & McCormick, P. G. (1990). Displacement Reactions during Mechanical Alloying, *Metallurgical Transaction A*, 21, 2789–2794.

[18] Forrester, J. S. & Schaffer, G.B. (1995). The chemical kinetics of mechanical alloying, *Metallurgical Transaction A*, 26, 725–730.

[19] Chicinas, I. (2006). Soft magnetic nanocrystalline powders produced by mechanical alloying routes. *Journal of Optoelectronics and Advanced Materials*, 8(2), 439–448.

[20] Arana, M., Jacobo, S. E., Troiani, H. & Bercoff, P. G. (2013). Synthesis and characterization of carbon-coated magnetite for functionalized ferrofluids, *IEEE Transactions on Magnetics*, 49(8), 4547–4550.

[21] Hisa M., Tsutsumi A. & Akiyama T. (2004). Reduction of iron oxides by nano-sized graphite particles observed in pre-oxidized iron carbide at temperatures around 873 K. *Materials Transaction*, 45(6), 907–910.

[22] Arana, M., Galván, V., Jacobo, S. E. & Bercoff, P. G. (2013). Cation distribution and magnetic properties of LiMnZn ferrites. *Journal of Alloys and Compounds*, 568, 5–10.

[23] Han, D. H., Wang, J. P. & Luo, H. L. (1994). Crystallite size effect on saturation magnetization of fine ferrimagnetic particles. *Journal of Magnetism and Magnetic Materials*, 136, 176–182.

[24] Chantrell, R. W., Popplewell, J. & Charles S. W. (1978). Measurements of particle-side distribution parameters in ferrofluids. *IEEE Transaction on Magnetics*, 14, 975–977.

[25] Shanhu, L., Feng, L., Ruimin, X., & Jun-Jie, Z. (2011). Structural effects of Fe_3O_4 nanocrystals on peroxidase-like activity *Chemistry A European Journal*, 17(2), 620–625.

[26] Cheng–Hao, L., Cheng–Ju, Y. & Wei-Lung, T. (2012). Fluorescence assay of catecholamines based on the inhibition of peroxidase–like activity of magnetite nanoparticles. *Analytica Chimica Acta*, 745, 143–148.

[27] Jianbo, L., Xiaona, H., Shuai, H., Tao, W., Wenqi, L., Xing, Z., Jun-Jie, Y. & Xiaochun, W. (2012). Au@Pt core/shell nanorods with peroxidase- and ascorbate oxidase–like activities for improved detection of glucose. *Sensors and Actuators B,* 166–167, 708–714.

[28] Chen, Z., Yin, J. J., Zhou, Y. T., Zhang, Y., Song, L., Song, M., Hu, S. & Gu, N. (2012). Dual enzyme–like activities of iron oxide nanoparticles and their implication for diminishing cytotoxicity. *ACS Nano*, 6(5), 4001–4012.

[29] Ai–Xian Z., Zhong-Xiao, C., Jin-Ru, W., Juan L., Huang-Hao,Y. & Guo-Nan, C. (2013). Highly–efficient peroxidase–like catalytic activity of graphene dots for biosensing. *Biosensors and Bioelectronics*, 49, 519–524.

[30] Patila M., Pavlidis, I. V., Diamanti, E. K., Katapodis P., Gournis D. & Stamatis H. (2013). Enhancement of cytochrome c catalytic behaviour by affecting the heme environment using functionalized carbon-based nanomaterials. *Process Biochemistry*, 48(7), 1010–1017.

[31] Teymourian H., Salimi A. & Khezrian S. Fe_3O_4 magnetic nanoparticles/reduced graphene oxide nanosheets as a novel electrochemical and bioeletrochemical sensing platform. (2013). *Biosensors and Bioelectronics*, 49, 1–8.

[32] Xiaoying N., Yinyin X., Yalei D., Liye Q., Shengda Q., Hongli C. & Xingguo C. (2014). Visual and quantitative determination of dopamine based on $Co_xFe_{3-x}O_4$ magnetic nanoparticles as peroxidase mimetics. *Journal of Alloys and Compounds*, 587, 74–81.

[33] Rodríguez, M. C. & Rivas, G. A. (2001). Highly selective first generation glucose biosensor based on carbon paste containing copper and glucose oxidase. *Electroanalysis*, 13 (14), 1179–1184.

[34] Luque, G. L., Rodríguez, M. C. & Rivas, G. A. (2005). Glucose biosensors based on the immobilization of copper oxide and glucose oxidase within a carbon paste matrix. *Talanta*, 66*,* 467–471.

[35] Erden, P. E., Zeybek, B., Pekyardımc, Ş. & Kılı, E. 2013. Amperometric carbon paste enzyme electrodes with Fe3O4 nanoparticles and 1,4-Benzoquinone for glucose determination. *Cells, Nanomedicine, and Biotechnology*, 41, 165–171.

[36] Lin M. S. & Leu H. J. 2005. A Fe_3O_4-based chemical sensor for cathodic determination of hydrogen peroxide. *Electroanalysis*, 17(22), 2068–2073.

[37] Kamin, R. A. & Wilson, G. S. (1980). Rotating ring-disk enzyme electrode for biocatalysis, cinetic studies and characterization of the immobilized enzyme layer. *Anal. Chem*., 52, 1198-1205.

[38] Sampath, S. & Lev, O. (1996). Inert metal-modified, composite ceramic–carbon, amperometric biosensors: renewable controlled reactive layer. *Anal. Chem*. 1996, 68, 2015–2021.

Natia D.